



Numerical Modelling of Molten Carbonate Fuel Cell: Effects of Gas Flow Direction in Anode and Cathode

Tay C. L.^{1*} and Law M. C.²

¹Chemical Engineering Department, School of Engineering and Science, Curtin University Sarawak, Miri, Sarawak, Malaysia

²Mechanical Engineering Department, School of Engineering and Science, Curtin University Sarawak, Miri, Sarawak, Malaysia.

ABSTRACT

The modelling of a three-dimensional (3-D) molten carbonate fuel cell (MCFC) was developed to study the effects of gas flow direction (co-flow and counter-flow) in anode and cathode on the generated power density by solving the mass and momentum conservation equations, electrochemical reaction and heat transfer. The simulation result of the co-flow temperature distribution was compared with the experimental data obtained from open literature. The molar fraction distribution of gases in the anode and cathode gas channels and temperature distribution across the cell were compared between two different flow directions. Furthermore, the performance of MCFC, which operates in the temperature range of 823 - 1023 K, was analysed by comparing the generated power density. The results showed that MCFC with co-flow attained higher power density compared to that of counter-flow at 873 K. However, at higher temperature of 1023 K, the generated power density was the same for both gas flow directions.

Keywords: Counter flow, Heat transfer, Molten Carbonate Fuel Cell, Numerical simulation, Three-dimensional model

INTRODUCTION

Nowadays, various types of molten carbonate fuel cell (MCFC) have been commercialized to generate electricity of around 200 kW to

one megawatt for manufacturing factories, research centres, hospitals and commercial buildings (Ma *et al.*, 2009). The modelling of MCFC has become an important analysis method to better understand and optimize the operating conditions in order to improve its performance and lifespan.

According to Munoz *et al.* (2011), voltage calculation of MCFC could be categorised into three major approaches. The first approach was derived from the models developed for

Article history:

Received: 28 September 2013

Accepted: 18 January 2014

Email addresses:

Tay C. L. (taycl@curtin.edu.my),

Law M. C. (m.c.law@curtin.edu.my)

*Corresponding Author

solid oxide fuel cells (SOFC), which combined the experimental and theoretical approach; the second approach looked into the electrodes kinetics based on Butler-Volmer equation which was first developed by Yuh and Selman (1989), and the third approach focused on the voltage losses at cathode based on the Arrhenius-type equations (Baranak & Atakul, 2007).

He and Chen (1995) developed a 3-D, 5-cells stack model with a thickness of 14 mm for each cell and electrochemical area size of 1 m². The temperature and pressure distributions at the operating temperature of 873 K for three different gas flow types (co-flow, cross-flow and counter-flow) have been reported. Kim and co-workers (2010) developed a 3-D MCFC with corrugated gas channels and studied the current density distribution, ohmic resistance, and anode and cathode polarizations for three different gas flow directions at the operating temperature of 853 K. It was reported that the counter-flow model gave the best performance due to its smaller ohmic resistance and electrodes polarization.

The operating temperature of MCFC is in the range of 873 - 973 K and the maximum temperature gradient over the cells is recommended not to exceed 90 K in order to maintain the lifespan of the cells (Huppmann, 2009). It is believed that the high operating temperature may cause hot corrosion of current collector and separator, creep or compaction of electrodes and electrolyte matrix, as well as electrolyte loss that could reduce the lifespan of cells (Yuh & Farooque 2009). However, a low operating temperature may decrease the cell power density due to high ohmic resistance and electrodes polarization. The modelling of the MCFC is vital in achieving the balance between its performance and lifespan by optimising its operating condition and efficiency.

In the current study, a 3-D single cell MCFC model was developed using commercial software, COMSOL (version 4.1). This model solves a set of Navier-Stokes equations which includes multi-component gas species and Yuh and Selman's model (1984), which is used for the voltage-current relationship. The result of the temperature distribution was compared with the literature data. The effects of gas flow direction in the anode and cathode gas channels on the generated power density at different operating temperatures were also studied using the developed model.

MODELLING APPROACH

The modelling of MCFC was carried out based on several assumptions. Due to the symmetry of MCFC, only a pair of cathode and anode gas channels was simulated. The gas in the anode and cathode was assumed to be an ideal gas mixture, and the flow is laminar. The carbonate ions diffusion across the electrolyte was assumed to have a negligible effect on the performance of MCFC.

There are six main components in MCFC: current collectors, anode gas channel, anode electrode, electrolyte, cathode electrode and cathode gas channel (see Fig.1). The size of MCFC is 4.5 mm (W) × 7.0 mm (H) × 140 mm (D). The model contains 12800 elements, with 10 grids in the width direction for the fuel and oxidant channel. Details for the six main components are shown in Table 1.

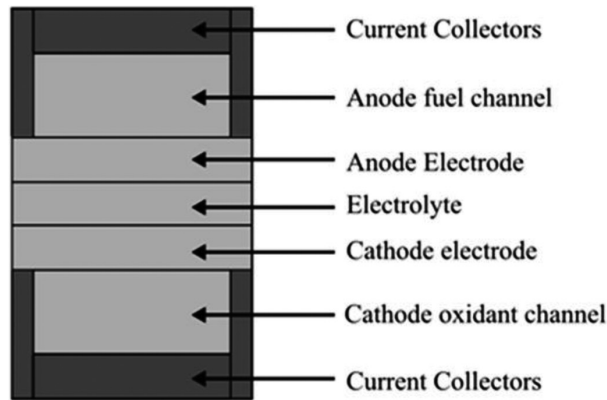
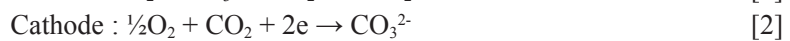
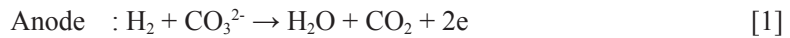


Fig.1. Front view of the MCFC 3-D model

TABLE 1
Specification of the components of MCFC cell (Yu *et al.*, 2008)

Components	Thickness (mm)	Porosity (%)	Mesh grids
Current collectors	0.8		3
Anode fuel channel	1.5		7
Anode electrode	0.8	0.5	5
Electrolyte	0.8		10
Cathode electrode	0.8	0.55	5
Cathode oxidant channel	1.5		7

The electrochemical reactions in MCFC’s electrodes are shown as follows:



Based on the overall reaction, the electrons, carbonate ions are conserved within the overall reactions [3]. The carbonate ions, CO_3^{2-} , are consumed in the anode and generated in the cathode at the same reaction rate. The chemical reactions are presumed to occur in the electrode domains. The exterior surfaces of MCFC are adiabatic. In the counter-flow model, the flow direction in anode fuel channel remained the same but the flow direction in cathode oxidant channel is the opposite of that of fuel flow.

The oxidant and fuel in the channels are governed by the, single phase, laminar Navier-Stokes equations:

$$\nabla \cdot (\rho u) = Sp \quad [4]$$

$$\rho(u \cdot \nabla)u = \nabla \cdot \left[-\rho I + \mu(\nabla u + (\nabla u)^T) - \frac{2}{3}\mu(\nabla \cdot u)I \right] \quad [5]$$

where, ρ is the pressure (Pa), u is the velocity vector (m/s), I is the identity matrix, and T is the temperature (K). In the gas channels, the mass source term, S_p , is zero.

For the porous anode and cathode electrodes, the gas phase momentum is described by Darcy equation:

$$\frac{\rho}{\epsilon_p} \left((u \cdot \nabla) \frac{u}{\epsilon_p} \right) = \nabla \cdot \left[-\rho I + \frac{\mu}{\epsilon_p} (\nabla u + (\nabla u)^T) - \frac{2\mu}{3\epsilon_p} (u \cdot \nabla) I \right] - \frac{\mu u}{\kappa_{br}} \quad [6]$$

where, ϵ_p is the porosity, μ is dynamic viscosity (Pa·s) and κ_{br} is the permeability (m²).

The rate of production/destruction of each species, S_j (mol/m³s) in anode and cathode electrodes is:

$$S_j = v_j \frac{i}{2F\delta} MW_j \quad [7]$$

where v_j is stoichiometric constant for a gas species j , i is electrical current density (A/m²), F is Faraday constant (96485.3 C/mol), MW_j is molecular weight of a gas species j (g/mol) and δ is the thickness (m).

The source terms in the anode and cathode electrodes are shown as follows (Kim *et al.*, 2010):

$$\text{Anode: } S_p, \text{ anode} = S_{CO_2} + S_{H_2} - S_{H_2} \quad [8]$$

$$\text{Cathode: } S_p, \text{ cathode} = -(S_{CO_2} + S_{O_2}) \quad [9]$$

The transport of these concentrated gas species is described as:

$$\nabla \cdot J_j + \rho(u \cdot \nabla)\omega_j = S_j \quad [10]$$

where, ω_j is the mass fraction of a gas species of j , and J_j is defined by a mixture-average equation:

$$J_j = - \left(\rho D_j^m \nabla \omega_j D_j^m \frac{\nabla M_n}{M_n} \right) \quad [11]$$

where, the D_j^m is the mixture-average diffusion coefficient and M_n is defined as:

$$M_n = \left(\sum_j \omega_j / M_j \right)^{-1} \quad [12]$$

The heat transfer of MCFC is described with convection and conduction mechanisms as:

$$\rho C_p u \cdot \nabla T = \nabla \cdot (k_{eq} \nabla T) + Q \quad [13]$$

where, C_p is specific heat capacity at constant pressure (J/(kg·K)), k_{eq} is the thermal conductivity (W/(m·K)) and Q is total heat source.

The total heat generated from MCFC was calculated by adding the electrical energy and the enthalpy change of the overall reaction [3] above (Koh *et al.*, 2002).

$$\text{Energy source : } Q = [-r\Delta H + V_{cell}i] \frac{1}{\delta} \quad [14]$$

where r is the reaction rate, (mol/m²s), ΔH is molar enthalpy (J/mol), V_{cell} is electric voltage (V).

The molar enthalpy of formation of water was calculated as:

$$\Delta H = -(240506 + 7.3835T) \quad [15]$$

The cell potential of the MCFC depends on the thermodynamic reversible potential, partial pressure of fuel gases and oxidant gases in the electrodes, and the irreversible losses of the cell due to the limits of the electrical current and the kinetic rate (Yuh & Selman, 1984).

$$V_{cell} = E_{rev} - i(\eta_a + \eta_c + \eta_{ohm}) \quad [16]$$

where E_{rev} is derived from the Nernst equation that considering the partial pressure of fuel gases in anode and oxidant gases in cathode (Kim *et al.*, 2010).

$$E_{rev} = E^0 + \frac{RT}{2F} \ln \frac{P_{H_2}^a}{P_{H_2O}^a \cdot P_{CO_2}^a} + \frac{RT}{2F} \ln \left(\sqrt{P_{O_2}^c P_{CO_2}^c} \right) \quad [17]$$

The ideal standard potential E^0 for the cell reaction is calculated from Koh *et al.* (2002):

$$E^0 = 1.2723 - 2.7645 \times 10^{-4} \times T \quad [18]$$

The ohmic loss ($\Omega \text{ m}^2$) is the electrical resistance caused by current flow (Kim *et al.*, 2010).

$$\eta_{ohm} = 0.5 \times 10^{-4} \exp \left[3016 \left(\frac{1}{T} - \frac{1}{923} \right) \right] \quad [19]$$

The activation polarization of anode and cathode (Yuh & Selman, 1984):

$$\eta_a = 2.27 \times 10^{-9} \exp \left[\frac{6435}{T} \right] \times P_{H_2}^{-0.42} \times P_{CO_2}^{-0.17} \times P_{H_2O}^{-0.1} \quad [20]$$

$$\eta_c = 7.505 \times 10^{-10} \exp \left[\frac{9298}{T} \right] \times P_{O_2}^{-0.43} \times P_{CO_2}^{-0.09} \quad [21]$$

The operating and boundary condition of MCFC are shown in Table 2.

TABLE 2
Operating and boundary conditions of MCFC (Yu *et al.*, 2008)

Parameter	Value
Operating pressure	101,325 Pa
Operating temperature	873 K
Current density	1400 A/m ²
Inlet mole fraction of fuel gases in the anode, H ₂ :CO ₂ :H ₂ O	0.40 : 0.40 : 0.20
Inlet mole fraction of oxidant gases in the cathode, O ₂ :CO ₂ :N ₂	0.148 : 0.296 : 0.556
Anode inlet gas flow rate	40 litre/min
Cathode inlet gas flow rate	112.7 litre/min

RESULTS AND DISCUSSION

In Fig.2, it was observed that the temperature of the co-flow model increased from 873 K at the cathode inlet to the maximum temperature of 923 K at the cathode outlet. However, the temperature profile for the counter-flow is different compared to that of co-flow, where the temperature of the counter-flow model increases from 873K to 888K at the middle of the cell and decreases to 876K towards the end of the cell. This temperature profile could be due to the heat energy in cathode oxidant channel was regulated by the lower temperature from the anode inlet of MCFC. This happened to the anode side as well, whereby, the high temperature at the outlet of anode was regulated by the lower temperature at the cathode inlet of counter-flow model.

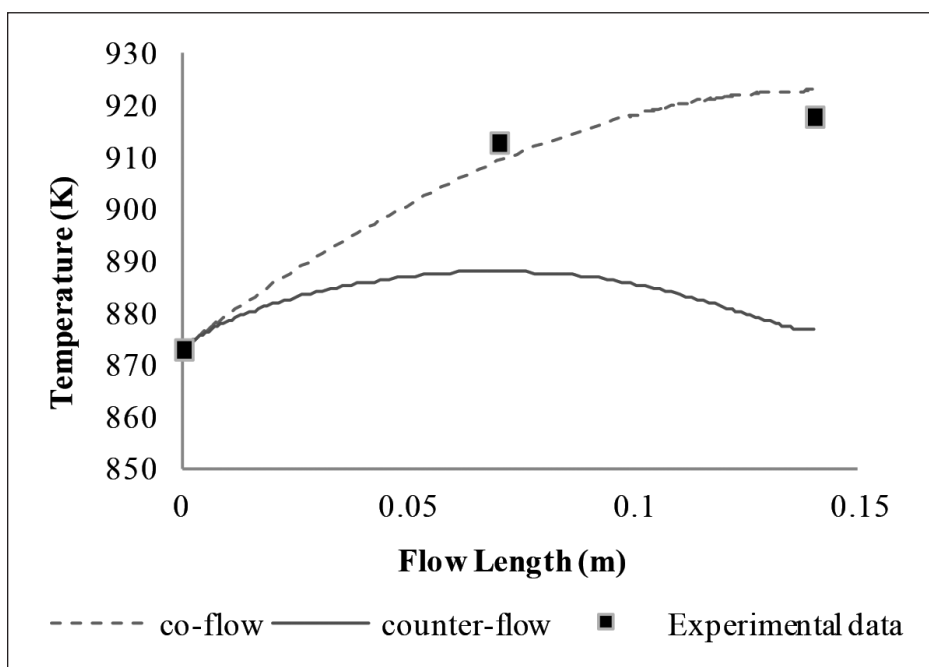


Fig.2. Temperature distributions of co-flow and counter-flow models operated at 873 K

The developed MCFC model has been validated with the literature data by comparing the temperature distribution across the cathode oxidant fuel channel (Yu *et al.*, 2008). By comparing the result with the published experimental result, it was found that there are 0.44% temperature difference at the middle of the cell and 0.54 % temperature difference at the end of the cell (see Fig.2). The temperature differences were in the range of ± 5 K. The developed model was considered valid to further study the effects of the gas flow direction in the anode fuel channel and cathode oxidant channel.

Fig.3 and Fig.4 show the comparison for the distribution of hydrogen and water vapour in the anode fuel channel and the distribution of carbon dioxide and oxygen in the cathode oxidant fuel channel between two different gas flow models. From the figures, the reactant consumption and product formation rates for both models are the same from the inlet to the outlet of the cell. This result was supported with equation [7], whereby the rate of production/destruction of each gas species in the anode and cathode was not temperature-dependent.

The performances of the MCFC cell for two different gas flow directions were analysed by comparing the generated power density from temperature of 823 K to 1023 K (Fig.5). It was observed that the MCFC cell with co-flow attained higher performance compared to the counter-flow model at a lower temperature. As the temperature increased from 823 K to 1023 K, the generated power density was also increased. However, the performances of the MCFC cell for these two flow configurations got closer at the temperature of 973K and became the same at 1023K.

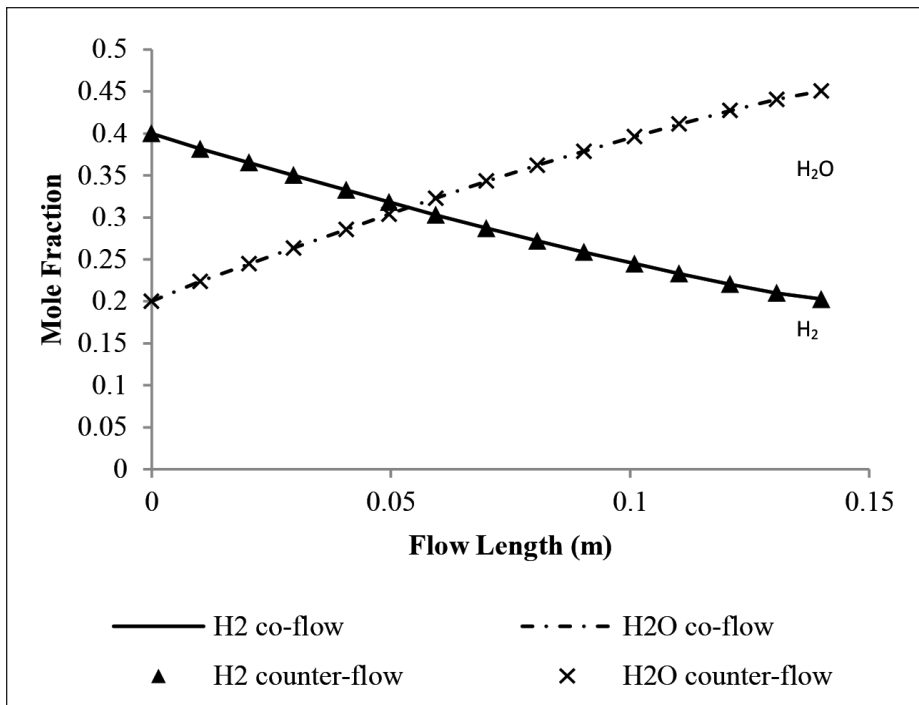


Fig.3. Distributions of hydrogen and water vapour in anode fuel channel of co-flow and counter flow models

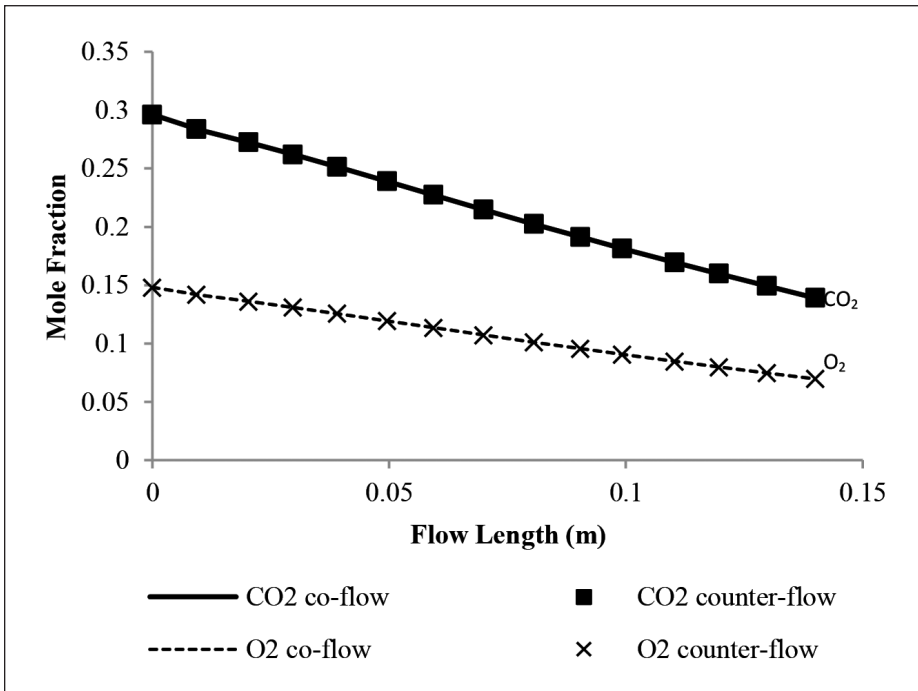


Fig.4. Distributions of oxygen and carbon dioxide in cathode oxidant channel of co-flow and counter-flow models

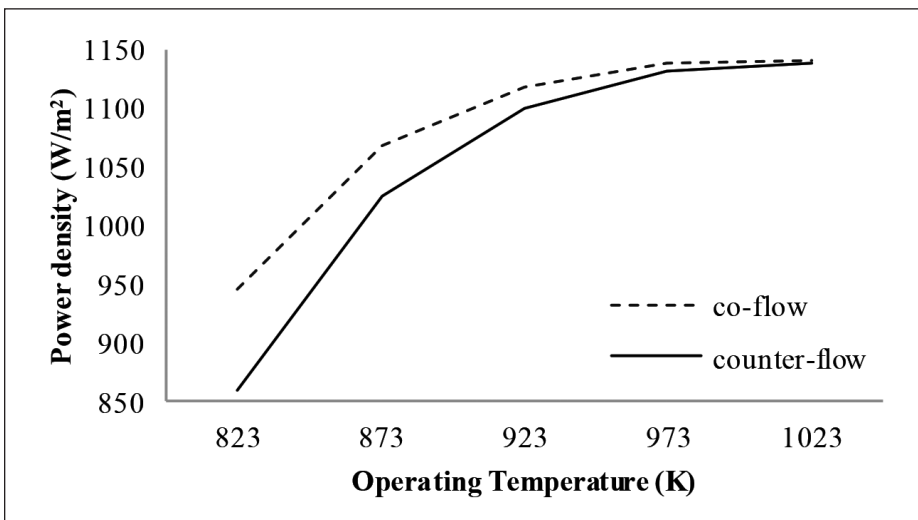


Fig.5. Generated power densities of co-flow and counter-flow models at various temperatures

The different performances of the co-flow and counter-flow models can be investigated through the overall cell voltage and total voltage losses due to the Nernst loss, ohmic loss, cathode and anode activation losses (Eqn. [19]-[21]). By comparing the voltage loss for the different gas flow models at 873 K, it was observed that cathode activation loss for the co-flow is 30% lower as compared that of counter-flow (Fig.6). Cathode and anode activation losses contributed to a high percentage of total voltage losses for the counter-flow model, which caused the lower overall cell voltage and lower power density, compared to the co-flow model. The higher cathode activation loss for the counter-flow model was caused by the lower temperature distribution across the inlet and outlet of the cathode oxidant channel as mentioned above. The relationship of the temperature and the cathode activation polarization was explained in equation [21]. At the temperature of 873 K, the co-flow model attained a higher overall cell voltage of 0.7596 V as compared to that of counter-flow model, which was 0.7331 V. Higher overall cell voltage contributed to higher generated power density at constant current output.

At the operating temperature of 973 K, the co-flow model produced a higher overall cell voltage of 0.8132 V as compared to counter-flow model, which was 0.8021 V. The differences of the overall cell voltage were small as compared to the different gas flow models that operated at the temperature of 873 K. The total voltage losses for both co-flow models operated at 873 K (Fig.6) and 973 K (Fig.7) were reduced as compared to counter-flow models, especially the for the cathode and anode activation losses. It is believed that the higher temperature distribution from the cathode inlet to the outlet of the co-flow models was the main reason for the dramatically reduction of the cathode activation loss (Fig.8).

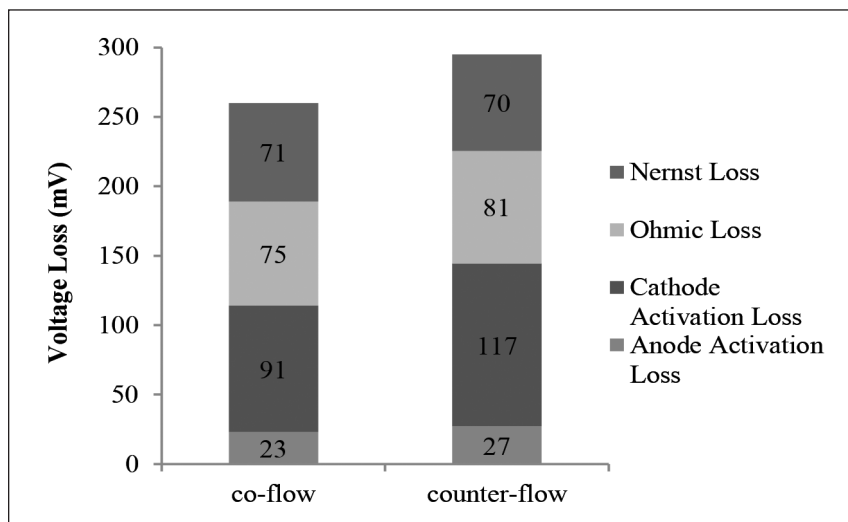


Fig.6. Voltage losses of co-flow and counter-flow models operated at 873 K and average current density of 1400 A/cm²

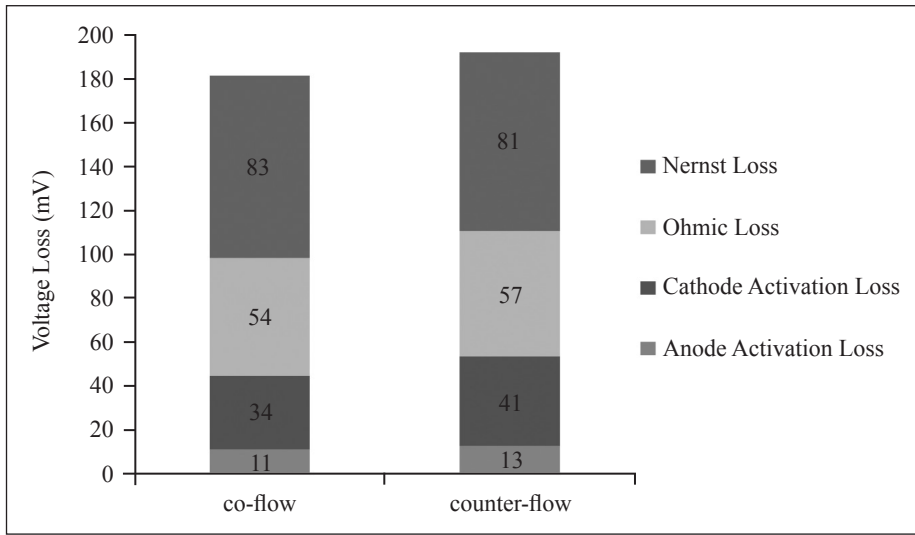


Fig.7. Voltage losses of co-flow and counter-flow models operated at 973 K and average current density of 1400 A/cm²

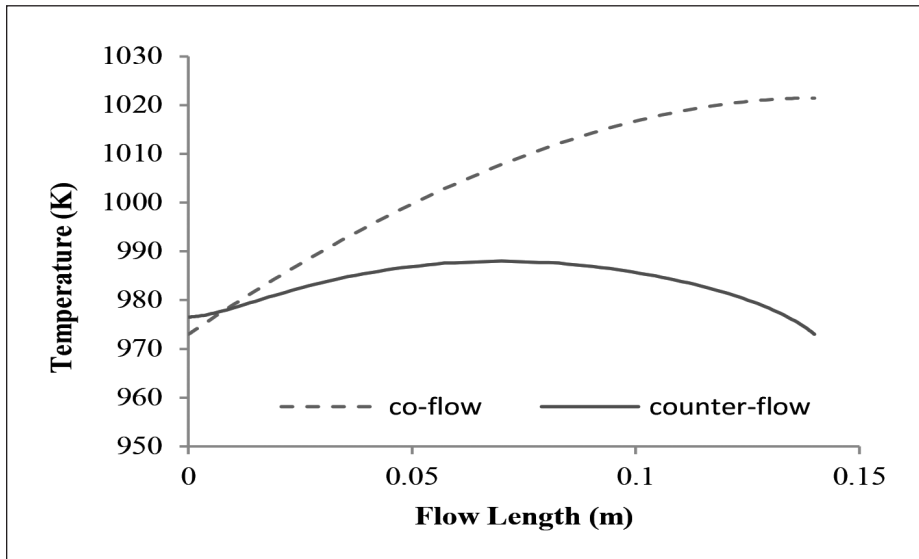


Fig.8. Temperature distributions of co-flow and counter-flow models operated at 973 K

CONCLUSION

The co-flow model was found to have a higher performance as compared to the counter-flow model because of the higher temperature distribution across the cathode inlet to the outlet. The lower temperature distribution of the counter-flow model was caused by the heat regulation from the lower temperature of both anode and cathode inlets. The higher temperature

distribution has the advantages in reducing the total voltage loss especially in the reduction of cathode and anode activation losses. By reducing the total voltage losses, the overall cell voltage and generated power density was increased. It is suggested that the co-flow model is suitable for the MCFC to be operated at lower temperatures of 823-923K to generate a higher power density. The counter-flow MCFC model is more appropriate for MCFC operated at temperature of 923-973K to generate high power density and at the same time maintaining the lower temperature profiles.

ACKNOWLEDGMENTS

The authors acknowledge the Sarawak Energy Berhad, Malaysia, for sponsoring the licenses of COMSOL 4.1 Multiphysics engineering simulation software and Curtin Sarawak, Malaysia, for the High Performance Computer facilities.

REFERENCES

- Baranak, M., & Atakul, H. (2007). A basic model for analysis of molten carbonate fuel cell. *Journal of Power Sources*, 72, 831 - 839.
- He, W., & Chen, Q. (1995). Three-dimensional simulation of a molten carbonate fuel cell stack under transient conditions. *Journal of Power Sources*, 55, 25 - 32.
- Huppmann, G. (2009). Fuel cells – molten carbonate fuel cells | Systems. In J. Garche (Ed.), *Encyclopedia of Electrochemical Power Sources* (p. 479 - 496). Amsterdam: Elsevier.
- Kim, Y. J., Chang, I. G., Lee, T. W., & Chung, M. K. (2010). Effects of relative gas flow direction in the anode and cathode on the performance characteristics of a Molten Carbonate Fuel Cell. *Fuel*, 89, 1091 - 1028.
- Koh, J. H., Seo, H. K., Yoo, Y. S., & Lim, H. C. (2002). Consideration of numerical simulation parameters and heat transfer models for a molten carbonate fuel cell stack. *Chemical Engineering Journal*, 87, 367 - 379.
- Ma, Z., Venkataraman, R., & Farooque, M. (2009). Fuel cells – molten carbonate fuel cells | Modeling. In J. Garche (Ed.), *Encyclopedia of Electrochemical Power Sources* (pp. 519 – 532). Amsterdam: Elsevier.
- Munoz de Escalona, J. M., Sanchez, D., Chacartegui, R., & Sanchez, T. (2011). A step-by-step methodology to construct a model of performance of molten carbonate fuel cells with internal reforming. *International Journal of Hydrogen Energy*, 36, 15739 - 15751.
- Yu. L. J., Ren, G. P., & Jiang, X. M. (2008). Experimental and analytical investigation of molten carbonate fuel cell stack. *Energy Conversion & Management*, 49, 873 - 879.
- Yuh, C., & Farooque, M. (2009). Fuel cells – molten carbonate fuel cells | Materials and Life Considerations. In J. Garche (Ed.), *Encyclopedia of Electrochemical Power Sources* (pp. 497 506). Amsterdam: Elsevier.
- Yuh, C. Y., & Selman, J. R. (1984). Polarization of the molten carbonate fuel cell anode and cathode. *Journal of The Electrochemical Society*, 131, 2062 - 2068.

